

THESIS FOR THE DEGREE OF MASTER OF SCIENCE

# Molecular dynamics simulations of proton diffusion in yttrium doped barium zirconate

JAKOB FRIMAN



**CHALMERS**

*Department of Applied Physics*  
CHALMERS UNIVERSITY OF TECHNOLOGY  
Gothenburg, Sweden 2013

Molecular dynamics simulations of proton diffusion in yttrium doped barium zirconate

JAKOB FRIMAN

©JAKOB FRIMAN, 2013

Department of Applied Physics  
Chalmers University of Technology  
SE-412 96 Göteborg  
Sweden  
Telephone + 46 (0)31-772 1000

Printed at Chalmers Reproservice  
Göteborg, Sweden 2013

## **Abstract**

Yttrium doped barium zirconate is a promising candidate as a proton conducting fuel cell electrolyte. Even if the mechanism behind proton conductivity is generally understood, the effects of dopants is a question that requires clarification. Recent studies suggests that dopants might act as traps for protons. An increased understanding of the behavior of protons in the vicinity of dopant atoms might contribute to the performance of future electrolytes.

The aim of this thesis is to investigate the possibilities of studying proton diffusion with the means of molecular dynamics simulations, using the ReaxFF potential as the model for the inter atomic interactions. The work includes a study of the thermal expansion of yttrium doped barium zirconate, the diffusion of protons and how to obtain the self intermediate scattering function, which can be measured with neutron scattering experiments.

The ReaxFF potential seems to provide a good model for studying proton diffusion in barium zirconate and it reproduces experimental results quite accurately. It is possible to obtain the self intermediate scattering function and study the motion of protons at different time and length scales. An exponential function, containing three parameters, were fitted to the obtained data. More investigations are required to interpret the data accurately, but some indication of the trapping effects of dopants can be seen.



## Acknowledgements

I owe my greatest thanks to my supervisor, professor **Göran Wahnström**, for suggesting and guiding me through this thesis, I have learned a lot of interesting things. I owe many thanks to **Anders Lindman** for doing the DFT calculations, for interesting discussions and answering many of my questions, to **Mattias Slabanja** for his patience and his guidance in the *dynsf* program, to **Anton Johansson** for his help during the construction of some of the MATLAB programs I have used during this thesis, to **Martin Petisme**, **Shiwu Gao**, **Paul Erhart**, **Edit Helgee** and **Hugo Strand** for answering questions and helping me with LAMMPS, time and time again, to **Arno Fey** for helping me with *vmd* and to **Adri van Duin** for providing the ReaxFF potential.

To my parents, **Eva** and **Edward**, I would like to extend my many thanks and undying gratitude for your never swaying support, I feel that I can always count on you. I want to thank all my friends for all the fun during my studies and free time here at Chalmers, and all other places.

*Jakob Friman*

Chalmers, Soliden lvl 3

March 1 2013



# Nomenclature

## Abbreviations

DFT Density Functional Theory

LAMMPS Large-scale Atomic/Molecular Massively Parallel Simulator

MD Molecular Dynamics

MSD Mean Square Displacement

PCSO Proton Conducting Solid Oxide

PEM Polymer Electrolyte Membrane

s-CF Self Correlation Function

s-ISF Self Intermediate Scattering Function

SOFC Solid Oxide Fuel Cell

## Elements

Ba Barium

H Hydrogen

O Oxygen

Y Yttrium

Zr Zirconium

## Symbols

$\ddot{\mathbf{r}}_i$  Acceleration of particle  $i$

$\Delta G$  Change in Gibbs free energy

---

$\Delta H$	Change in enthalpy
$\Delta S$	Change in entropy
$\Delta t$	Time step
$\nu$	Frequency
$\Omega$	Simulation volume
$\omega$	Angular frequency
$\mathbf{F}_i$	Force acting on particle $i$
$\mathbf{k}$	Momentum
$\mathbf{r}_i$	Position of particle $i$
$\mathbf{r}_i(t)$	Position of particle $i$ at time $t$
$\mathbf{v}_i(t)$	Velocity of particle $i$ at time $t$
$BO_{ij}$	Bond order between atom $i$ and $j$
$D$	Self diffusion constant
$d$	Effective lattice parameter
$D_0$	Prefactor
$E_0$	Activation energy
$F(\mathbf{k},t)$	Intermediate scattering function
$F_s(\mathbf{k},t)$	Self Intermediate Scattering Function
$G(\mathbf{r},t)$	Correlation function
$G_s(\mathbf{r},t)$	Self correlation function
$h$	Planck's constant, $4.1356675 \cdot 10^{-5}$ eVs
$K$	Equilibrium constant
$k$	Absolute value of momentum
$k_B$	Boltzmann's constant, $8.6173324 \cdot 10^{-5}$ eVK $^{-1}$
$L$	Side length of the simulation volume
$m_i$	Mass of particle $i$
$N$	Number of particles

---

$N_A$	Avogadro's number, $6.022 \cdot 10^{23} \text{ mol}^{-1}$
$p_{\text{H}_2\text{O}}$	Partial pressure of water
$R$	Gas constant, $8.3144621 \text{ Jmol}^{-1}\text{K}^{-1}$
$r$	Absolute value of distance
$r_c$	Cutoff distance
$r_{ij}$	Distance between particle $i$ and $j$
$S(\mathbf{k},\omega)$	Scattering function
$S_s(\mathbf{k},\omega)$	Self scattering function
$t$	Time
$V$	Inter atomic potential
$T$	Temperature

# Contents

<b>Nomenclature</b>	<b>i</b>
<b>1 Introduction</b>	<b>1</b>
1.1 Thesis Outline . . . . .	2
<b>2 Working Principles of a Fuel Cell</b>	<b>3</b>
2.1 Anode . . . . .	4
2.2 Cathode . . . . .	4
2.3 Over All Reaction . . . . .	4
<b>3 Barium Zirconate</b>	<b>7</b>
3.1 Perovskite Structure . . . . .	7
3.2 Protonation . . . . .	7
3.2.1 Dopant Atoms and Protonic Defects . . . . .	8
3.2.2 Chemical Equilibrium and Protonic Defect Concentration . . . . .	9
3.3 Proton Diffusion . . . . .	10
3.3.1 Effects of Dopants and Octahedral Tilting . . . . .	11
<b>4 Molecular Dynamics Simulations</b>	<b>13</b>
4.1 Basic Molecular Dynamics Theory . . . . .	13
4.1.1 The MD Method . . . . .	13
4.1.2 Inter Atomic Potentials . . . . .	14
4.1.3 System Size and Boundary Conditions . . . . .	15
4.1.4 Thermostats and Barostats . . . . .	16
4.1.5 A MD Simulation Program . . . . .	17
4.2 The ReaxFF Potential . . . . .	18
4.2.1 Very Short Description of Density Functional Theory . . . . .	19
<b>5 Analyzing Proton Diffusion</b>	<b>21</b>
5.1 Correlation Functions . . . . .	21
5.1.1 Mean Square Displacement . . . . .	21

5.1.2	Intermediate Scattering Function . . . . .	22
5.2	Analysis Software . . . . .	24
<b>6</b>	<b>Results</b>	<b>25</b>
6.1	Comparison Between the ReaxFF Potential and DFT . . . . .	25
6.2	Expansion of Yttrium Doped Barium Zirconate . . . . .	26
6.2.1	Lattice Parameter . . . . .	26
6.2.2	Distortions From the Cubic Lattice Structure . . . . .	30
6.3	Proton Diffusion in Yttrium Doped Barium Zirconate . . . . .	31
6.3.1	Mean Square Displacement . . . . .	31
6.3.2	Self Intermediate Scattering Function . . . . .	34
<b>7</b>	<b>Discussion</b>	<b>37</b>
<b>8</b>	<b>Conclusions</b>	<b>39</b>
	<b>Bibliography</b>	<b>42</b>



# 1

## Introduction

CLEAN ENERGY ALTERNATIVES have become more and more important during the last decades. One of these clean energy alternatives is the fuel cell. A fuel cell is a device that converts chemically stored energy into electrical energy[1]. There are several types of fuel cells and they are each suited for different tasks. Some of the main differences between various types of fuel cells are the fuels used, operating temperatures and the conducting ions.

The solid oxide fuel cell (SOFC) or ceramic fuel cell is a high temperature fuel cell that operates at temperatures of about 750 – 1000°C. The name Solid Oxide Fuel Cell originates from the fact that the electrolyte is a solid oxide, generally yttria-stabilized zirconia that conducts oxygen vacancies. The fuel can be a mixture of hydrogen and carbon monoxide or methane. Due to these high operating temperatures many requirements need to be fulfilled by the materials used for the SOFC. Other problems related to the high operating temperature are long start up times and casing/storage issues[2],[3].

The polymer electrolyte membrane (PEM) fuel cell is a low temperature fuel cell that has typical operating temperature around 80°C. The electrolyte of a PEM fuel cell is a proton conducting polymer and requires hydrogen as fuel. The PEM fuel cell needs platinum catalysts to work and is subjected to CO-poisoning, it therefore requires expensive fuel converter to create pure hydrogen gas free from CO. There are a number of other types of low temperature fuel cells with similar problems[2].

Because of these problems, with existing fuel cells, a lot of research has and is being made to reduce the operating temperature of the SOFC. The aim of today's research is to reach operating temperatures of about 500 – 700°C, also called the intermediate temperature range[3]. A reduction of the operating temperatures would decrease the material requirements and cost of the fuel cell without introducing the need for expensive catalysts. One way to reduce the operating temperatures is to change or modify the electrolyte. A promising alternative is to use proton conducting solid oxides (PCSO) that have a relatively high ionic conductivity of about  $10^{-2}$  S/cm at the desired temperatures.

There are however some problems connected to the PCSO. Some of the PCSO:s have a tendency to react with the carbon dioxide in the atmosphere for the desired temperatures, and decompose to form carbonates. Another problem is that some of the PCSO:s are not protonated in the intermediate temperature range. Barium zirconate is one of the PCSO:s that shows the highest proton conductivities. Yttrium doped barium zirconate is stable and protonated for temperatures in the intermediate temperature range, it is considered to be one of the most promising electrolytes for a future proton conducting SOFC[4].

Even if yttrium doped barium zirconate is considered to be one of the best alternatives as an electrolyte in the proton conducting SOFC, it can still be improved. The basic mechanism for proton conductivity is relatively well known but the effects of grain boundaries and dopants still require more investigation. An increased understanding of these effects might contribute to the work on improving the properties of the PCSO:s. Both experimental and computer based techniques are used to investigate the conduction mechanisms of the PCSO:s. Recent studies[5] suggests that dopant atoms acts as traps for protons, which means that protons spends an extended amount of time around the lattice sites of the dopant atoms compared to the time they spends at other sites in the lattice.

The ability to use computational results instead of (or parallel to) experiments is something that has developed more and more during the last centuries[6]. This of course has to do with the increased computational power of newer computers and the desire to understand physical mechanisms on the atomic scale. Molecular dynamics (MD) simulations are, as the name suggests, a way to simulate the behavior and interaction of particles on the atomistic scale, usually a few Ångströms, using computers.

The purpose of this thesis is to investigate the possibility to model proton diffusion in yttrium doped barium zirconate at finite temperatures using MD. The aim is to obtain the *self intermediate scattering function*, which can be measured experimentally with neutron scattering. To perform MD simulations, the inter atomic interactions must be known, for this purpose the ReaxFF potential[7], developed by van Duin *et al*, is used. The MD simulations are done using Large-scale Atomic/Molecular Massively Parallel Simulator (LAMMPS)[8].

## 1.1 Thesis Outline

This report contains three main parts. First a theoretical background is given, where the concept of fuel cells are described in chapter 2 and then a more detailed description of barium zirconate follows in chapter 3. The second part describes molecular dynamics simulations, chapter 4 explains the concept and chapter 5 describes how the results can be analyzed. The third part contains the results, which are presented in chapter 6, discussed in chapter 7 and finally some conclusions are given in chapter 8.

# 2

## Working Principles of a Fuel Cell

FUEL CELLS CONVERTS chemically stored energy into electrical energy. Fuel cells only converts energy and this makes them different from batteries that both stores and converts energy. As mentioned in the introduction there are many types of fuel cells. This chapter will explain the working principles of a fuel cell with protons as the conducting ions. For information about other types of fuel cells, see references[1][9].

The working principle of a hydrogenic fuel cell are very straight forward. Hydrogenic refers to that hydrogen gas is used as fuel. Se figure 2.1 for a sketch of a hydrogenic fuel cell. Below follows a brief description of reactions that takes place in the anode and cathode. The electrolyte will be addressed in chapter 3.

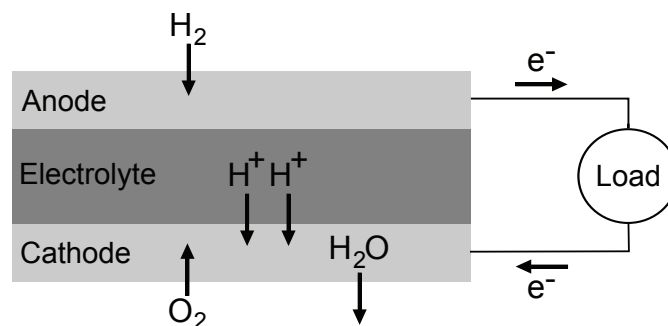


**Figure 2.1:** A simple schematic of a fuel cell with a proton conducting electrolyte. The hydrogen is dissociated at the anode, the protons diffuse through the electrolyte and the electrons travels through the external circuit. Protons and electrons reacts with oxygen at the cathode and forms water.

## 2.1 Anode

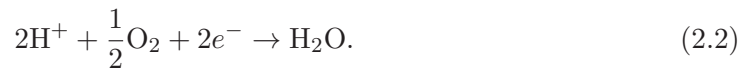
Hydrogen gas ( $\text{H}_2$ ) is transported to the anode of the fuel cell where the molecules are dissociated into protons ( $\text{H}^+$ ) and electrons ( $e^-$ ). The anode is made from a porous material to allow for as much contact with the fuel and electrolyte as possible. The dissociation is achieved in different ways depending on the type of fuel cell that is used. In high temperature fuel cells the high temperature is an important contribution in the dissociation of hydrogen. Low temperature fuel cells requires expensive catalysts like platinum to lower the energy barrier for dissociation[9]. The reaction in the anode is described by



The electrons travel through the external circuit to the cathode while the protons diffuse through the electrolyte.

## 2.2 Cathode

The cathode is in contact with air or more specifically oxygen gas ( $\text{O}_2$ ). The cathode, like the anode, needs to be porous to enable as much contact as possible with the air and electrolyte. The oxygen reacts with the protons from the electrolyte and the electrons from the external circuit. The reaction produces water ( $\text{H}_2\text{O}$ ) and to remove it the cathode need to have hydrophobic properties. The low temperature fuel cells also need catalysts in the cathode to lower the energy barrier of the reaction[9]. The reaction in the cathode is described by



## 2.3 Over All Reaction

The over all reaction in the fuel cell is described by the simple expression



The electrical power is extracted from the external circuit where the electrons produce a current.

It is rather straight forward to calculate the voltage of the fuel cell by studying the reaction in equation 2.3. The energy released in the reaction is  $\Delta H = 286 \text{ kJ}$  and the entropy is  $\Delta S = 163 \text{ J/K}$  for room temperature[10]. By assuming that the enthalpy and entropy are temperature independent, Gibbs free energy can be calculated using

$$\Delta G = \Delta H - T\Delta S, \quad (2.4)$$

for some temperature  $T$  in the intermediate temperature range.

For  $T = 800\text{ K}$  the change in Gibbs free energy is  $\Delta G = 156\text{ kJ/mol}$ . There are two electrons released for each reacting molecule of hydrogen  $\text{H}_2$ , so by dividing with Avogadro's number  $N_A$ , times two, and dividing by the electron charge, the energy per electron becomes  $0.81\text{ eV}$ , which is  $0.81\text{ V}$  per electron. This is the maximum voltage that can be obtained per electron and this can be compared to the maximum voltage  $1.23\text{ V}$  per electron at room temperature. As seen from the above calculation, the maximum voltage decreases for higher temperatures and there are several other factors that decreases it even further. As a result, the use of stacks of fuel cells, connected in series, is a common way to increase the voltage to be able to use the fuel cell technology in more energy consuming applications.



# 3

## Barium Zirconate

THERE ARE MANY mechanisms and issues related to the diffusion of protons in barium zirconate but everything except for the bulk mechanisms are beyond the scope of this thesis. This chapter describes the structure, the way in which protons are integrated and the physical mechanisms behind the diffusion of protons in the bulk of barium zirconate. In the end of the chapter a description of the possible reasons behind the trapping of protons close to dopants is given.

### 3.1 Perovskite Structure

Barium zirconate has a so called perovskite structure which is defined by that the oxygen atoms form an octahedral structure around the zirconium atoms. The lattice is cubic and it is there for called a cubic perovskite structure. An image of a unit cell with lattice partameter  $a$  in the barium zirconate crystal can be seen in figure 3.1. The cyan atoms are barium, the yellow one is zirconium and the red ones are oxygen. The chemical formula for barium zirconate is  $\text{BaZrO}_3$  and a general formula for perovskite oxides is  $\text{ABO}_3$ .

Another way to describe the perovskite structure is to picture it as a combination of  $bcc$  and  $fcc$  lattices. In this case the barium atom sits at the  $(0,0,0)$  site known as the A site in the unit cell, the zirconium atom sits at the "bcc site" known as the B site and the oxygen at the "fcc" sites. The picture with  $bcc$  and  $fcc$  sites is however not entirely correct because the octahedral structures are tilted in comparison to each other when compared over multiple unit cells[11]

### 3.2 Protonation

To be able to use barium zirconate as an electrolyte it needs to be protonated, which means that protons need to be integrated into the structure[12][13]. The reason for

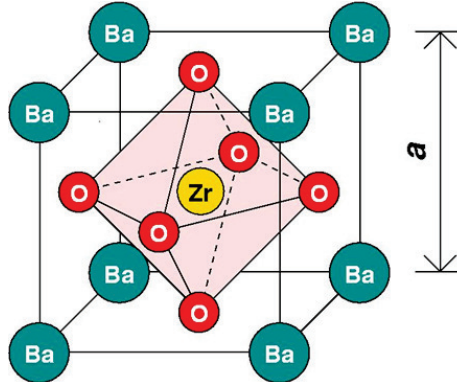


**Figure 3.1:** The perovskite structure in a unit cell of barium zirconate with lattice parameter  $a$ . The cyan atoms are barium, the yellow one is zirconium and the red ones are oxygen

protonating the material is to increase the number of charge carriers while still keeping the material neutrally charged. If barium zirconate without integrated protons were to be used as electrolyte, no protons would enter the electrolyte due to the fact that it would increase its energy. By protonating the material the reactions at the anode and cathode will add and remove protons at the same rate and thereby sustaining the process of proton conduction.

### 3.2.1 Dopant Atoms and Protonic Defects

Barium (Ba) has a formal ionic charge of 2+, zirconium (Zr) has 4+ and oxygen (O) has 2-. By replacing some of the zirconium atoms with atoms that has an ionic charge of 3+, in this case yttrium (Y), the system becomes charged. To equilibrate for this charge the system creates oxygen vacancies ( $V_{\text{O}}^{\bullet\bullet}$ ), so for every two dopant atoms one oxygen atom is removed. The system is now yttrium doped barium zirconate which has the formula  $\text{BaZr}_{1-\alpha}\text{Y}_{\alpha}\text{O}_{3-\frac{\alpha}{2}}$ , where  $\alpha$  is the concentration of yttrium[4][11].

If the system is in a humid atmosphere, water molecules will dissociate into protons ( $\text{H}^+$ ) and hydroxide ions ( $\text{OH}^-$ ). The hydroxide ion fills an oxygen vacancy and the proton forms a covalent bond with one of the neighboring oxygen atoms in the lattice. These pairs of an oxygen atom and a proton are positively charged and are called protonic defects ( $\text{OH}_{\text{O}}^{\bullet}$ )[4]. The chemical reaction for formation of protonic defects is described by



The notation is called Kröger-Vink notation[13], a  $\bullet$  denotes a positive charge, a  $x$  denotes a neutral charge, a  $'$  denotes a negative charge and the subindex, O in this case, denotes which lattice position the species occupies.

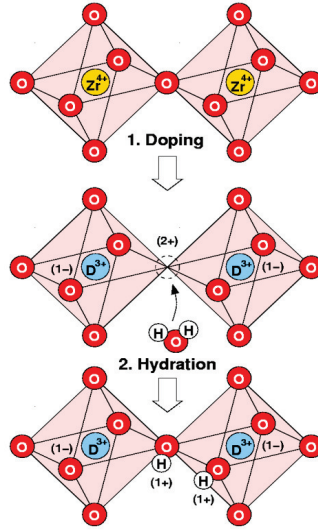


**Figure 3.2:** The protonation process. barium zirconate is doped with yttrium that replaces some of the zirconium atoms. The yttrium charge is less than the zirconium charge and this creates oxygen vacancies that can absorb water and introduce protons into the structure.

The system is now in what is called a hydrated state, it is still neutrally charged but has protons integrated in the structure. A schematic over the protonation process is shown in figure 3.2.

### 3.2.2 Chemical Equilibrium and Protonic Defect Concentration

The reaction in equation 3.1 goes in both directions. Chemical equilibrium refers to when the concentration of reactants (left hand side) and products (right hand side) are constant. An equilibrium constant can be defined by

$$K = \exp\left(\frac{\Delta G}{RT}\right) = \exp\left(\frac{\Delta S}{R}\right) \exp\left(\frac{-\Delta H}{RT}\right) = \frac{[\text{OH}_\text{O}^\bullet]^2}{[\text{V}_\text{O}^{\bullet\bullet}][\text{O}_\text{O}^x]p_{\text{H}_2\text{O}}}, \quad (3.2)$$

where the brackets in the third equality denotes the concentration of each species and  $p_{\text{H}_2\text{O}}$  is the partial pressure of water. The equilibrium constant can also be described with thermodynamical quantities by using the first and second equalities, where  $R$  is the gas constant[4][13].

The neutral charge or electroneutrality condition can be described by

$$2[\text{V}_\text{O}^{\bullet\bullet}] + [\text{OH}_\text{O}^\bullet] = [\text{Y}'_{\text{Zr}}] = \text{constant}, \quad (3.3)$$

where  $[\text{Y}'_{\text{Zr}}]$  denotes the concentration of negatively charged yttrium dopants at zirconium sites.

By assuming that

$$[\text{O}_\text{O}^x] + [\text{OH}_\text{O}^\bullet] + [\text{V}_\text{O}^{\bullet\bullet}] = [\text{O}] = \text{constant}, \quad (3.4)$$

in molar concentration  $[\text{O}] = 3$ , and using the electroneutrality condition in equation 3.3, the concentration of protonic defects can be described by

$$[\text{OH}_\text{O}^\bullet] = \frac{[\text{O}]Kp_{\text{H}_2\text{O}} \left( -1 + \sqrt{1 - \frac{2[\text{Y}'_{\text{Zr}}]}{[\text{O}]} + \frac{[\text{Y}'_{\text{Zr}}]^2}{[\text{O}]^2} + \frac{8[\text{Y}'_{\text{Zr}}]}{Kp_{\text{H}_2\text{O}}[\text{O}]} - \frac{4[\text{Y}'_{\text{Zr}}]^2}{Kp_{\text{H}_2\text{O}}[\text{O}]^2}} \right)}{4 - Kp_{\text{H}_2\text{O}}} \quad (3.5)$$

[13].

### 3.3 Proton Diffusion

Protonic defects are hydroxide ions and the oxygen and the proton are bound together via a strong covalent bond, but due to that the proton is positively charged, it can form weaker hydrogen bonds with neighboring oxygen atoms[13]. Barium zirconate is one of the perovskites with the largest lattice parameter, 4.19 Å at room temperature[14][15], so the proton will be attracted by the nearest neighboring oxygen ions and the covalent bond will be parallel with the octahedral edges, which are shown as black lines in figure 3.1. For perovskites with small lattice parameters the proton is more attracted to the second nearest neighbors due to the repulsion from the strongly positive zirconium ions at the B sites. Because of the attraction between the proton and it's oxygen neighbors a contraction of the oxygen lattice occurs around the proton[13].

In order for the proton to diffuse it must break the bonds to the surrounding oxygen atoms. The hydrogen bonds are weak and easily broken so the proton will move around between the neighboring oxygen atoms, forming and braking hydrogen bonds while keeping the covalent bond intact. This will result in a rotational motion in a "donut shaped" pattern with the covalently bonded oxygen atom at the center. The reason that the hydrogen bond is so easily broken is because of that the free energy gained by forming the bond is counteracted by the loss of free energy due to the lattice distortion when the oxygens are pulled towards the proton[13].

For long range proton diffusion to occur, the covalent bond must be broken. This happen relatively easy for a straight line bond configurations of  $O - H \cdots O$ , where  $-$  denotes a covalent bond and  $\cdots$  a hydrogen bond, but the hydrogen bond is bent because of the repulsion from the positive ions. This has the effect that in order for the proton to "jump" it must go through both an energy and momentum transfer. When the breaking and formation of covalent bond actually occurs, the configuration  $O - H \cdots O$  is almost linear but for this to happen the bond between the oxygen and the B site ion,  $B - O$ , has to be elongated, reducing the repulsion between the hydrogen and the B site ion. When this happen a contribution to the system energy arises from the stretching of the  $B - O$  bond. The resulting activation energy for long range proton diffusion has contributions from both the  $B - O$  stretching and the proton transfer barrier, and for cubic perovskite-type oxides it is of the order of 0.4 – 0.6 eV[13].

The diffusion of protons in barium zirconate can be characterized by two diffusion rates[16], the rate at which the proton forms new hydrogen bonds with the neighboring oxygen ions and the rate at which the proton forms new covalent bonds or jumps to another oxygen ion. These events occur at different rates, the formation of new hydrogen bonds being faster than the formation of new covalent bonds. The diffusion of protons in barium zirconate can be seen as a random walk, with the rate of formation of new covalent bonds being the determining factor in the total rate of diffusion.

Long range proton diffusion can be described by

$$D = D_0 \exp\left(-\frac{E_0}{k_B T}\right) \quad (3.6)$$

[13] when considering long distances, which means that the distance the proton has moved from its starting position approaches infinity. The self diffusion constant  $D$  describes the quadratic displacement of the proton per unit time, common units are  $\text{cm}^2/\text{s}$ .  $D_0$  is a prefactor that depends on geometry, number of neighboring oxygen atoms the proton can jump to,  $O-O$  distance and the frequency with which the proton tries to jump to another oxygen.  $E_0$  is the activation energy discussed above,  $k_B$  is Boltzmann's constant. The diffusion constant increases with increasing temperature, this is because of the increased energy in the system which has the result that the energy barriers are more easy to overcome.

### 3.3.1 Effects of Dopants and Octahedral Tilting

As mentioned earlier the octahedral structures of oxygen in barium zirconate are a bit tilted, creating differences in the distance to the nearest neighbor oxygens, making some of the proton jumps easier, or more difficult, than others. This is illustrated in two dimensions in figure 3.3, where the red dots are oxygen atoms in two tilted octahedra. If a proton has a covalent bond with oxygen 1, it is harder to jump to oxygen 2 than oxygen 3, since distance A is longer than distance B.

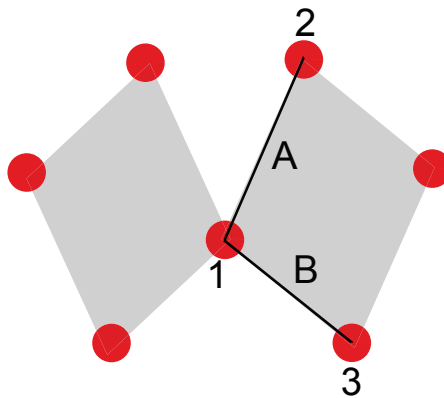


**Figure 3.3:** Two dimensional illustration of two tilted octahedra, the red dots are oxygen atoms. If a proton has a covalent bond with oxygen 1, it is harder to jump to oxygen 2 than oxygen 3, since distance A is longer than distance B.

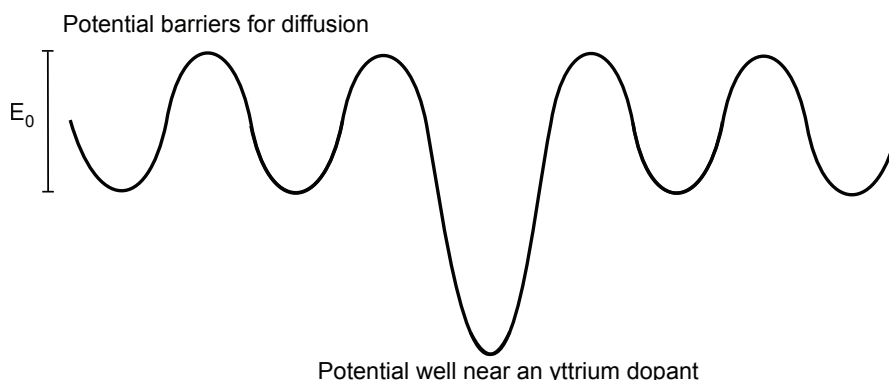


**Figure 3.4:** The traps near the yttrium dopant's can be seen as dips in the potential landscape.

In some perovskites the tilting can lead to a chain of shorter jump distances after each other creating a path along which the proton diffuses more easily, making the diffusion anisotropic[13]. In undoped barium zirconate the tilting averages out over longer distances making the long range diffusion isotropic.

The yttrium ions has a considerably larger ionic radius than the zirconium ions. This leads to that when barium zirconate is doped with yttrium at the B sites, the larger ionic radius will create a distortion in the oxygen structure surrounding the yttrium atoms[11][13]. Earlier studies shows that these distortions have no effects on the diffusion of protons[13], but more recent studies suggests that the yttrium dopants might act as traps for the protons[5],[17], [18] and [19], and there by decreasing the diffusion. These traps can be seen as dips in the potential landscape, illustrated in figure 3.4.

When a proton has formed a covalent bond with one of the oxygens that is a trap, it will linger there for a longer time than it would at any "normal" oxygen because it is harder to overcome the energy barrier to the neighboring oxygen atoms. The reasons behind these traps are different for different dopants. In the case of yttrium there are mainly two reasons, one electrostatic related and one structure related[19].

The electrostatic attraction arises from that the yttrium dopants has a weaker positive ionic charge (3+) that the zirconium ions (4+). Due to this weaker ionic charge the repulsion between the dopants and the protons are weaker than the repulsion between the protons and the zirconium ions[19].

The structure related reason for trapping involves the oxygen sub lattice. Due to the large ionic radius of yttrium, the oxygen ions in the surrounding octahedron (O1) is pushed away from the yttrium ion towards the next nearest oxygen ions (O2), decreasing the distance between them. Because of this decreased distance, if a proton forms a covalent bond with one of the O2 ions it will be much easier for the proton to form a strong hydrogen bond with the O1 ion than any of the other surrounding oxygen ions, making it linger longer at the O2 site[19].

# 4

## Molecular Dynamics Simulations

**M**OLECULAR DYNAMICS SIMULATIONS can be used to investigate physical quantities that are difficult to measure in experiments. For example, it is relatively easy to track the movement of an individual atom, which otherwise requires advanced experimental set ups. It is of course important to compare the results between molecular dynamics (MD) simulations and experiments to check the validity of the models used[6]. This chapter explains some of the basic principles behind MD simulations and the most important steps in a MD simulation program. At the end of the chapter a brief description of the ReaxFF potential is given.

### 4.1 Basic Molecular Dynamics Theory

MD simulations are used to study the time evolution of classical systems. The word classical here refers to that the particles in the system are assumed to obey the laws of classical mechanics. This classical approximation is valid in most cases but for materials with lighter elements such as hydrogen or helium, quantum effects may need to be taken into account for lower temperatures or if the vibrational motion satisfies  $h\nu > k_B T$ , where  $h$  is Planks constant and  $\nu$  is the frequency of the motion[6].

#### 4.1.1 The MD Method

MD simulations can in short be described as time integration of Newton's equations of motion for the particles in the system[6]. To solve Newton's equation of motion the force  $\mathbf{F}_i$  acting on each particle needs to be known. To be able to calculate the forces it is necessary to have a description of the particle interactions in the system. The particle interactions are described by an interatomic potential  $V$  from which the force is obtained through

$$\mathbf{F}_i = -\nabla_i V, \quad (4.1)$$

[20] where the index  $i$  denotes which particle the force acts upon. The potential is dependent on the position of the particles,

$$V = V(\mathbf{r}_1, \mathbf{r}_2, \dots, \mathbf{r}_N), \quad (4.2)$$

where  $N$  is the number of particles and  $\mathbf{r}_1 \dots \mathbf{r}_N$  their respective positions. Newton's equation of motion

$$\mathbf{F}_i = m_i \ddot{\mathbf{r}}_i, \quad (4.3)$$

where  $m_i$  is the particle mass and  $\ddot{\mathbf{r}}_i$  the acceleration of the particle [20], can then be set up for each particle in the system  $i = 1, \dots, N$ , giving a set of coupled ordinary differential equations. Given a set of initial conditions for the positions  $\mathbf{r}_i(t)$  and velocities  $\mathbf{v}_i(t)$ ,

$$(\mathbf{r}_1(0) \dots \mathbf{r}_N(0), \mathbf{v}_1(0) \dots \mathbf{v}_N(0)), \quad (4.4)$$

at time  $t = 0$ , it is possible to iterate numerically in time and create a trajectory

$$(\mathbf{r}_1(t) \dots \mathbf{r}_N(t), \mathbf{v}_1(t) \dots \mathbf{v}_N(t)) \quad (4.5)$$

in time. With this information it is possible to calculate other observables. For example can the temperature for a classical system be calculated from the average kinetic energy of the particles [6].

### 4.1.2 Inter Atomic Potentials

There are many different types of potentials and the potential for a system can be produced in different ways. First a theoretical model is often used to determine the structure of the potential, which energy contributions that are taken into account and how they should be described. The energy contributions are parameterized and the parameters are fitted to data to obtain the actual values of the potential. The parameters can be fitted to either theoretical data like the one obtained from density functional theory (DFT), which will be shortly explained in section 4.2.1, or to experimental data.

The simplest type of potential is a so called pair potential, meaning that the interaction energy is pairwise additive. The energy for one particle can then be calculated by adding together the contributions from the interaction with the other particles and the total energy by doing this for all the particles in the system. If the interaction energy between two particles are given by  $v(r_{ij})$ , where  $r_{ij} = |\mathbf{r}_i - \mathbf{r}_j|$  is the distance between them, the total potential energy will be given by

$$V(\mathbf{r}_1, \mathbf{r}_2, \dots, \mathbf{r}_N) = \frac{1}{2} \sum_{i=1}^N \sum_{j \neq i} v(r_{ij}). \quad (4.6)$$

If the potential is more complicated more terms need to be added that are not pairwise additive and takes more particles and their relative positions into account.

### 4.1.3 System Size and Boundary Conditions

An important part in a MD simulation is the simulation volume in which the simulation takes place. The simulation volume plays an important part in defining the system. This is done via the boundaries and how they treat the volume outside of the simulation volume. The outside can be viewed as an empty space, in which case the particles inside of the simulation volume just interact with each other. This can be used when the system of interest is a cluster, a nanoparticle or another system that is small enough so that it can be contained within the simulation volume without making the computation too heavy. When simulating bulk materials there are no boundaries, which makes it impossible to fit the whole system into the simulation volume. If the simulation should treat a bulk system, a solution is to use periodic boundary conditions.

#### Periodic boundary conditions

Periodic boundary conditions means that the particles interact over the boundaries of the simulation volume. This will create a repetition of the simulation volume in all directions, which gives the illusion of an infinite system without boundaries. Using periodic boundary conditions just requires the computer to keep track of the particles inside of the simulation volume. Any particle position in one of the replicas can be calculated by using the information about the real particle position. A particle position  $\mathbf{r}_{\text{replica}}$  in one of the replicas can easily be calculated by

$$\mathbf{r}_{\text{replica}} = \mathbf{r}_{\text{real}} + \mathbf{n}L, \quad (4.7)$$

where  $\mathbf{r}_{\text{real}}$  is the particle position in the simulation volume,  $L$  the length of the side of the simulation volume, which for simplicity is assumed to be cubic, and  $\mathbf{n}$  is a three dimensional vector with integer components corresponding to in which replica of the simulation volume that  $\mathbf{r}_{\text{replica}}$  is in.

A general form of periodic boundary conditions would be that each particle in the simulation volume interacts with all the other particles in the simulation volume and all the particles in the replicas, including the particle's own replica. This general case is not possible in practice. A summation of all particle interactions would be an infinite sum, making the above approach impossible to implement. Also, the fact that particles interact with their own replicas will give rise to correlations.

In MD simulations, most of the interactions are short ranged, meaning that most of the interaction energy arises from interactions with neighboring particles inside of a cutoff distance  $r_c$ . A special case of interest is when  $r_c < L/2$ , leading to that particles just interact with the nearest replica of the other particles and never with it's own replica. This is illustrated in figure 4.1. Long range interactions need special treatment and how this is done depends on the system. Another important fact about periodic boundary conditions is that the simulation volume can be defined to be anywhere in the system of replicas, without the result of the simulation being changed, but it must have the same shape and orientation. This is an effect of that the infinite system is periodic over the

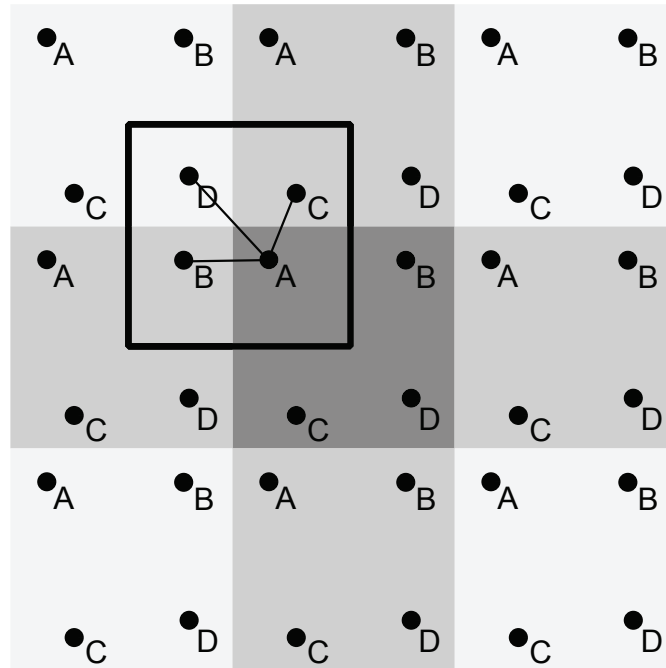


**Figure 4.1:** A two dimensional visualization of periodic boundary conditions. The darkest filled box in the middle is the simulation volume. The particles in the simulation volume interact with the nearest replicas of the other particles, creating the illusion of an infinite lattice. The simulation volume can be defined to be anywhere (black square) without the result of the simulation being changed, but it needs to have the same shape and orientation.

distance  $L$  in the direction of the boundaries. This is illustrated by the black square in figure 4.1.

#### 4.1.4 Thermostats and Barostats

Newton's equation of motion conserves the system energy. The temperature of a system can be calculated from the velocities of the particles in it. It is also possible to do the opposite, controlling the the temperature by modifying the equation of motion. This is done technically using a thermostat, which is a modification of Newton's equation of motion that rescales the velocities to obtain some given temperature. There are many different algorithms for how this can be done in practice. LAMMPS uses the Nose-Hoover thermostat, which is based on an extended Lagrangian method of formulating the equation of motion in classical mechanics and will not be discussed in more detail in this thesis. For the interested reader see references [6], [8] and [22] for a detailed explanation of the Nose-Hoover thermostat.

It is also possible to control the pressure during a MD simulation. The boundaries can be fixed if the system should be a specific size through out the whole simulation or they can be allowed to fluctuate, changing the size of the system. The later is used to to study the system under constant pressure, this is done using a barostat, which is a modification

of Newton's equation of motion that applies forces to the system boundaries and rescales the distances in the system. As with the thermostats there are many different algorithms for this purpose. The Nose-Hoover thermostat is also a barostat[8].

#### 4.1.5 A MD Simulation Program

There are some basic steps that need to be included in a MD simulation program. These steps can be summarized as follows:

1. Reading initial parameters
2. Initiation of the system
3. Calculation of the force on each particle
4. Time integration of the equation of motion
5. Write relevant data to output files
6. Repeat from step 3

##### Reading initial parameters

This is the step where the program takes input. Some input is always required regardless of the purpose of the simulation. Such input is the number of particles, particle positions, size of the system, boundary conditions, the potential and the time step  $\Delta t$  that determines the accuracy of the iterations forward in time. The user can add extra input depending on what is going to be simulated. This input can be environmental data like temperature or pressure.

##### Initiation of the system

The read input is now used to create atoms at the specified positions  $\mathbf{r}_i(0)$  in the simulation volume and giving them initial velocities  $\mathbf{v}_i(0)$  based on temperature if one has been specified. It is important to use realistic initial positions for the particles in the system. If particles overlap the forces on them will be very non realistic, leading to unwanted behavior. For example, very strong repulsive forces will cause the particles to accelerate extremely fast and lead to non physical behavior.

##### Calculation of the force on each particle

Knowing the system setup, the forces can be calculated on each particle. This part is often the most computationally heavy one depending on the potential. Often a particle interacts with many of its neighbors, requiring a summation over a lot of particle interactions for each particle. Some interactions are very long ranged, for example Coulomb interactions. These interactions require special treatment.

### Time integration of the equation of motion

When the forces are known they can be applied to the particles in the system, and new positions are obtained by moving forward in time. As with all numerical algorithms it is important to know that it is stable, that is the error does not increase over time. The stability is strongly related to the time step  $\Delta t$ . The time step should be kept small enough so that the algorithm is stable even for steep potentials.

### Write relevant data to output files

Relevant data can now be written to an output file that the user can later process with some suitable program. The output can be positions, velocities, instantaneous temperature or pressure and many other things. A file containing the particle coordinates for each time step is often referred to as a trajectory file. To save memory the relevant information should always be written to an output file so that the program does not have to remember old information during the entire run.

### Repeat from step 3

The procedure above is repeated for the number of time steps set by the user or until a specific condition is fulfilled. The way in which the number of steps is determined depends in the purpose of the simulation. When performing an energy minimization it is better to let the simulation stop when the energy change for each time step is smaller than some tolerance rather than running a certain amount of time steps, many enough to be sure that the energy has been minimized. If the simulation concerns a study of the dynamics a certain amount of time steps should be specified.

## 4.2 The ReaxFF Potential

The ReaxFF potential, developed by professor van Duin *et al*[7], is the potential used for the MD simulations in this thesis. The ReaxFF potential is a very complicated potential that includes a lot of parameters that has been fitted to data obtained from DFT calculations[7].

The ReaxFF potential is a so called many body potential, which means that it goes beyond the pair-potential description in section 4.1.2. One example of such a many body effect is the three particle interaction described by the angle between the atomic bonds.

One of the most important variables in the ReaxFF potential is the bond order. One of the notable assumptions in the ReaxFF potential is that the bond order  $BO_{ij}$  between two atoms can be determined from the distance  $r_{ij}$  between them, like in a pair potential. The different types of bonds the ReaxFF potential distinguishes between are sigma-bonds, pi-bonds and double pi-bonds. The bond order is used in many of the different energy terms.

Other notable energy contributions are the van der Waals and Coulomb interactions. These are the long range interactions that are calculated between all the atom pairs,

not just the bond sharing ones. These two energy terms also governs the repulsive Pauli principle at short distances even if the physical origin of the interactions are completely different.

#### 4.2.1 Very Short Description of Density Functional Theory

DFT is a way to work with quantum mechanical effects. Where a MD calculation just works with the atom - atom interactions a DFT calculation considers the electrons, their interactions with each other and with the nuclei. DFT is basically an approximate way to solve the Schrödinger equation for a many body system, but instead of working with electronic wave functions the DFT calculation works with electron densities and there by it's name. The calculation begins with an initial guess of the electron density and then an iterative procedure is performed during which the density is gradually changed until the lowest energy state is found. The electron density is described by a superposition of basis functions, which are often plane waves or Gaussian in shape. Electrons close to the core are highly localized and therefore require many basis functions to describe them, making the computation heavier. To avoid this, the electrons close to the core are often integrated into the potential that describes the core, creating a pseudopotential that is used instead[21].

DFT calculations are more accurate than interatomic potential descriptions but are much more computationally heavy, so it is only possible to treat systems several orders of magnitude smaller than those that can be treated with MD using an interatomic potential.



# 5

## Analyzing Proton Diffusion

**T**HE AIM OF this thesis is to study proton diffusion by the means of MD simulations. To investigate the diffusive motion, two different correlation functions were used, the mean square displacement (MSD) and the self Intermediate Scattering Function (s-ISF). This chapter describes the correlation functions that were used and some of the programs that were written during the thesis.

### 5.1 Correlation Functions

Here the two correlation functions are described and how they can be obtained from a MD trajectory.

#### 5.1.1 Mean Square Displacement

The MSD is the average squared displacement of particle  $i$  from an initial position  $\mathbf{r}_i(t_1)$  at time  $t_1$ , after a time  $t = t_2 - t_1$ , where the particle is at position  $\mathbf{r}_i(t_2)$  at time  $t_2$ . The MSD as a function of  $t$  is given by

$$MSD(t) = \langle |\mathbf{r}_i(t_2) - \mathbf{r}_i(t_1)|^2 \rangle = \langle r(t)^2 \rangle, \quad t = t_2 - t_1, \quad (5.1)$$

where  $\langle \dots \rangle$  denotes the time average over all  $t = t_2 - t_1$  and  $r$  is the absolute value of the displacement distance. To get even better statistics the average should also be taken over all identical particles  $N$  in the system, according to

$$MSD(t) = \frac{1}{N} \sum_{i=1}^N \langle |\mathbf{r}_i(t_2) - \mathbf{r}_i(t_1)|^2 \rangle, \quad t = t_2 - t_1. \quad (5.2)$$

For large times, the MSD approaches a linear function of time with the proportionality constant being related to the self diffusion constant according to

$$MSD(t) \rightarrow 6Dt, \quad \text{for large } t, \quad (5.3)$$

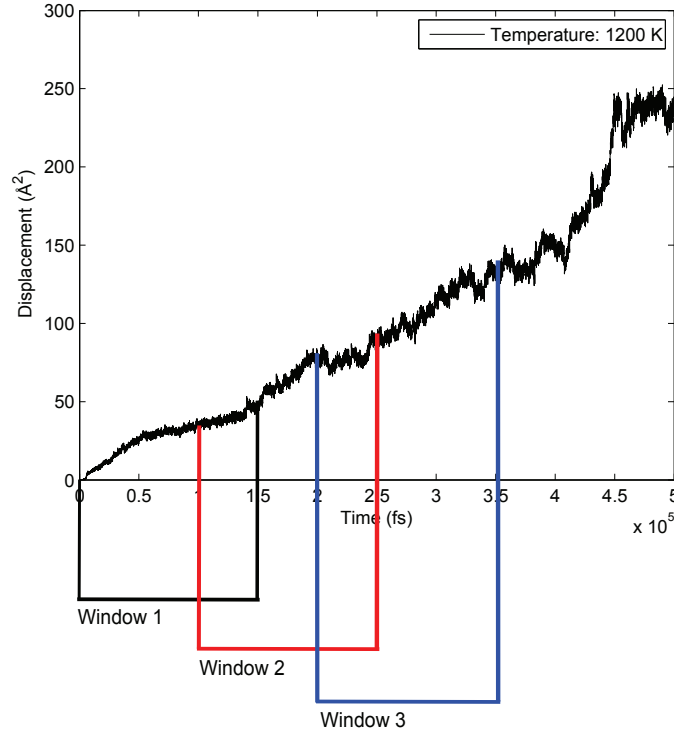


**Figure 5.1:** To get good statistics the MSD should be calculated for many different start positions  $t_1$ , but the time window  $t_2 - t_1$  should be kept constant.

where the factor 6 arises from the three dimensional geometry. For a detailed derivation of 5.3 see reference[23].

The MSD can easily be calculated from a trajectory. The squared displacement can be obtained from a trajectory file by starting at some position  $\mathbf{r}(t_1)$  at some time  $t_1$  and then calculate the squared change in coordinates from that position for each time step  $\Delta t$  to some later time  $t_2$ . To get the MSD the squared displacement should be averaged over many different start positions, but the time window  $t_2 - t_1$  should be kept constant. The concept of time windows is illustrated in figure 5.1 and denoted by the time average  $\langle \dots \rangle$  in equation 5.1. The diffusion constant can then be obtained from the slope of the curve  $MSD(t)$ .

### 5.1.2 Intermediate Scattering Function

More detailed information about the diffusive motion can be obtained by studying correlation functions in space and time.

The self correlation function (s-CF)  $G_s(\mathbf{r}, t)$  is the probability of finding a specific particle at position  $\mathbf{r}(t_2)$  at time  $t_2$  if that specific particle was at some position  $\mathbf{r}(t_1)$  at time  $t_1$ . The s-CF  $G_s(\mathbf{r}, t)$  can be written

$$G_s(\mathbf{r}, t) = \langle \delta(\mathbf{r} - (\mathbf{r}(t_2) - \mathbf{r}(t_1))) \rangle, \quad (5.4)$$

where the  $\langle \dots \rangle$  denotes the time average over all  $t = t_2 - t_1$ . Averaging over all identical particles gives

$$G_s(\mathbf{r}, t) = \frac{1}{N} \sum_{i=1}^N \langle \delta(\mathbf{r} - (\mathbf{r}_i(t_2) - \mathbf{r}_i(t_1))) \rangle. \quad (5.5)$$

The s-CF will have sharp peaks due to the delta functions at the starting positions of the particles at  $t = 0$ , but the peaks will broaden and decrease in height as time increases. This behavior is similar to that of the MSD but more detailed, because the self correlation function treats the positions in three dimensions.

In this thesis, the s-ISF is studied. The s-ISF  $F_s(\mathbf{k}, t)$  is the fourier transform

$$F_s(\mathbf{k}, t) = \int G_s(\mathbf{r}, t) e^{-i\mathbf{k} \cdot \mathbf{r}} d\mathbf{r} \quad (5.6)$$

in space of the s-CF  $G_s(\mathbf{r}, t)$ , where  $\mathbf{k}$  is the momentum. By using the fourier transform in equation 5.6, the s-ISF becomes

$$F_s(\mathbf{k}, t) = \frac{1}{N} \sum_{i=1}^N \langle e^{i\mathbf{k} \cdot (\mathbf{r}_i(t_2) - \mathbf{r}_i(t_1))} \rangle, \quad (5.7)$$

which can be calculated from a trajectory file by sampling the  $\mathbf{k}$ -vectors and then putting in the coordinate differences obtained from the file.

When considering small  $k$ -values and large times  $t$ , the fourier transform in equation 5.6 approaches an exponential form according to

$$F_s(\mathbf{k}, t) \rightarrow e^{-Dk^2 t}, \text{ for large } k \text{ and } t. \quad (5.8)$$

For a derivation of equation 5.8 see reference [23].

Having obtained the s-ISF, it is possible to do a fourier transform in time to obtain the self scattering function  $S_s(\mathbf{k}, \omega)$ , where  $\omega$  is the angular frequency.  $S_s(\mathbf{k}, \omega)$  can be used to directly measure the diffusion constant for small  $\omega$  and  $k$ [23], but this is not done in this thesis.

Another correlation function  $G(\mathbf{r}, t)$  can also be studied.  $G(\mathbf{r}, t)$  is the probability of finding any particle at position  $\mathbf{r}(t_2)$  at time  $t_2$  if there was any particle at position  $\mathbf{r}(t_1)$  at time  $t_1$ [23]. It is also possible to make fourier transforms of  $G(\mathbf{r}, t)$  in space and time, obtaining  $F(\mathbf{k}, t)$  and  $S(\mathbf{k}, \omega)$ .

The scattering function  $S(\mathbf{k}, \omega)$ , also called the structure factor, is often used to determine the structure of crystals via two fourier transforms to the correlation function  $G(\mathbf{r}, t)$ . The scattering function is often referred to as the coherent scattering function  $S(\mathbf{k}, \omega) = S_{Coh}(\mathbf{k}, \omega)$  while the self scattering function is the incoherent scattering function  $S_s(\mathbf{k}, \omega) = S_{Inc}(\mathbf{k}, \omega)$  and they can be measured with coherent and incoherent neutron scattering[23].

The reason that the s-ISF is of interest is that it can be measured directly via neutron scattering experiments using the spin-echo technique[5].

## 5.2 Analysis Software

The output files from LAMMPS are, in this thesis, either trajectory files containing the positions of all the protons for each time step or, in the case of thermal expansion, text files containing the size of the simulation volume for each time frame.

To analyze the trajectory files produced by LAMMPS, two different softwares were used, MATLAB[24] and dynsf[25]. MATLAB requires no further explanation but dynsf is less famous. dynsf is a program that can be used to calculate the s-ISF directly from a MD simulation trajectory. dynsf can calculate other observables as well, like the intermediate scattering function  $F(\mathbf{k},t)$ , scattering function  $S(\mathbf{k},\omega)$  or correlation function  $G(\mathbf{r},t)$ , but this was not done in this thesis.

One of the problems encountered when analyzing the data in the trajectory files is that the positions are "wrapped", this is an effect of periodic boundary conditions. "wrapped" refers to that if a particle leaves the simulation volume at one boundary it will, at the same time, be entered into simulation volume at the opposite boundary. This results in a jump in the particle's trajectory. To remedy this, an *unwrap* function was written in MATLAB. The *unwrap* function reads the original trajectory file, then calculates the positions that the particles would have if they had not been wrapped back into the simulation volume and then writes the new positions to a new trajectory file.

To calculate the diffusion constant from MSD, a MATLAB program was written that used the time window approach, mentioned in section 5.1.1, and also averaged over all the protons in the system.

To calculate the self ISF, both dynsf and MATLAB were used. dynsf was used to calculate the actual self ISF but some problems had to be addressed. First, the three dimensional  $\mathbf{k}$ -space is normally sampled with several thousand  $\mathbf{k}$ -points and the s-ISF is calculated for  $|\mathbf{k}| = k$ , this leads to a rather poor resolution for small  $k$ -values. To solve this the  $\mathbf{k}$ -space was uniformly sampled along the  $x,y$  and  $z$ -axis separately and then the average was taken between the three. This produces an evenly sampled  $\mathbf{k}$ -space for  $|\mathbf{k}|$ . This approach is possible because of that the diffusion of protons in barium zirconate is isotropic. Secondly,  $5 \cdot 10^6$  time steps, which was the length of the longest run, takes a very long time to process. This was solved using a logarithmic time scale, by first processing the first ten time frames, then each tenth time frame up to one hundred, then each hundredth up to one thousand time frames and so on. Each order of magnitude had to be treated separately. MATLAB was used to put together all of the different s-ISF:s created during the above mentioned approach.

# 6

## Results

THIS CHAPTER CONTAINS the results from the simulations and calculations performed during this thesis work. The three topics that were studied are the comparison of the ReaxFF potential that was used in all of the MD simulations to DFT calculations, the thermal expansion of yttrium doped barium zirconate and last the results of the main topic of interest, the proton diffusion in yttrium doped barium zirconate. All MD simulations were performed with LAMMPS[8].

### 6.1 Comparison Between the ReaxFF Potential and DFT

First a test was performed to investigate the reliability of the ReaxFF potential and how well it describes atomic configuration energies. The test was made through a comparison between the ReaxFF potential and DFT calculations.

The comparison was made by calculating the energy for seven different periodic structures, all with unit formula  $\text{Ba}_2\text{ZrYO}_6\text{H}$ . These structures are the same as the ones used in Ref. [7] by van Duin *et al.* It is not possible to compare the actual energies because they do not need to be the same. The force is calculated from the gradient of the potential so it is the energy difference between structures that is of importance. In order to be able to compare the energies, the energy of the first structure was subtracted from the other six, creating an energy difference that could easily be compared. The result can be seen in figure 6.1. The result shows that the ReaxFF potential differs from DFT calculated values with about 1 – 10 kJ/mol except for configuration 7 where the difference is around 40 kJ/mol.

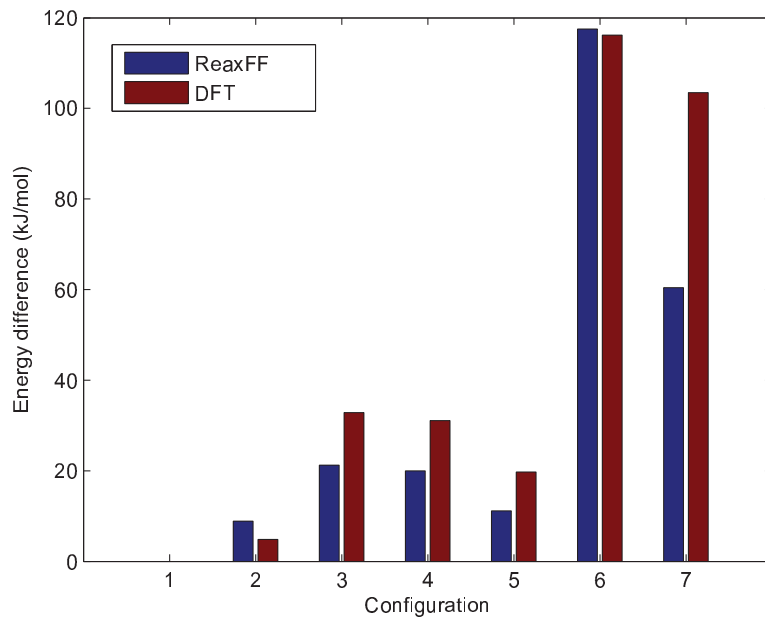


**Figure 6.1:** A comparison between the ReaxFF potential and DFT. Energy difference of six configurations of  $\text{Ba}_2\text{ZrYO}_6\text{H}$ , calculated using the ReaxFF potential, and DFT.

## 6.2 Expansion of Yttrium Doped Barium Zirconate

The expansion of yttrium doped barium zirconate was studied as a function of dopant concentration and temperature. The simulation volume contained  $6 \times 6 \times 6 = 216$  unit cells of  $\text{BaZrO}_3$ . Three yttrium dopant concentrations were studied,  $24/216$  parts yttrium  $\approx 11\%$ ,  $12/216$  parts yttrium  $\approx 6\%$  and no doping at all =  $0\%$ . The concentration was determined as  $[Y] + [Zr] = 1 = 100\%$ . The system was neutrally charged and fully protonated, including as many protons as yttrium dopants and no oxygen vacancies. Yttrium dopants and protons were randomly distributed in the simulation volume, yttrium dopants replacing some of the existing zirconium atoms and the protons were placed at any random coordinates. A relaxation of the lattice was then made to move the protons to physically possible locations and thereby avoiding atomic overlap.

The MD simulations were performed at constant temperature and constant pressure, always 1 atm, with a time step  $\Delta t = 1$  fs. Simulations were performed at 200 K, 400 K, 600 K, 800 K, 1000 K, 1200 K and 1400 K. For undoped barium zirconate, the temperature 1600 K was also studied.

### 6.2.1 Lattice Parameter

During the MD simulations the simulation volume was allowed to expand and contract under constant pressure and after a sufficient time, around 10 ps, an equilibrium was

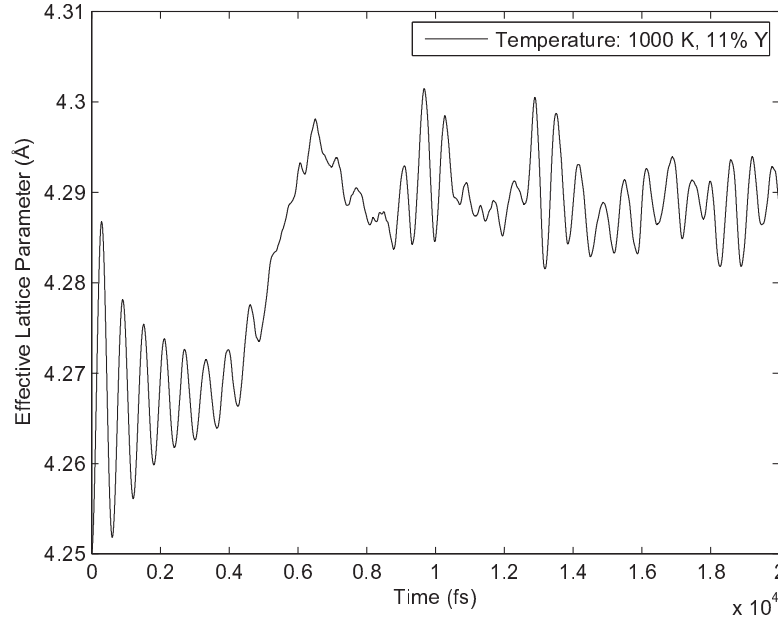


**Figure 6.2:** The lattice parameter as a function of time for constant pressure 1 atmosphere, at constant temperature 1000 K.

found. The simulation volume oscillates around the equilibrium, so the average was taken from  $t = 1.5 \cdot 10^4$  fs to the end of the simulation, giving an average simulation volume over the last 1/4 of the simulation. The effective lattice parameter  $d$  for one unit cell was then calculated from the simulation volume  $\Omega$  according to

$$d = \left( \frac{\Omega}{6^3} \right)^{\frac{1}{3}}. \quad (6.1)$$

The effective lattice parameter is calculated under the assumption of a cubic lattice, meaning that if the lattice is not cubic the effective lattice parameter will give the value of a cubic lattice with the same volume.

An example of a plot with effective lattice parameter as a function of time for constant temperature and pressure can be seen in figure 6.2. Figure 6.2 is the simulation performed at 1000 K with 11 % yttrium dopants, the lattice parameter starts at 4.25 Å and then starts to oscillate and between 4 ps and 6 ps the equilibrium of the oscillation changes to about 4.29 Å.

A MD simulation was carried out for each dopant concentration and temperature and the results are shown in figure 6.3.

From the results in figure 6.3 it is clear that the effective lattice parameter increases with temperature, as for most materials. The relation between the effective lattice parameter and temperature is almost linear for temperatures up to 1200 K, but a slight upward curvature can be seen. For the doped lattices the effective lattice parameter

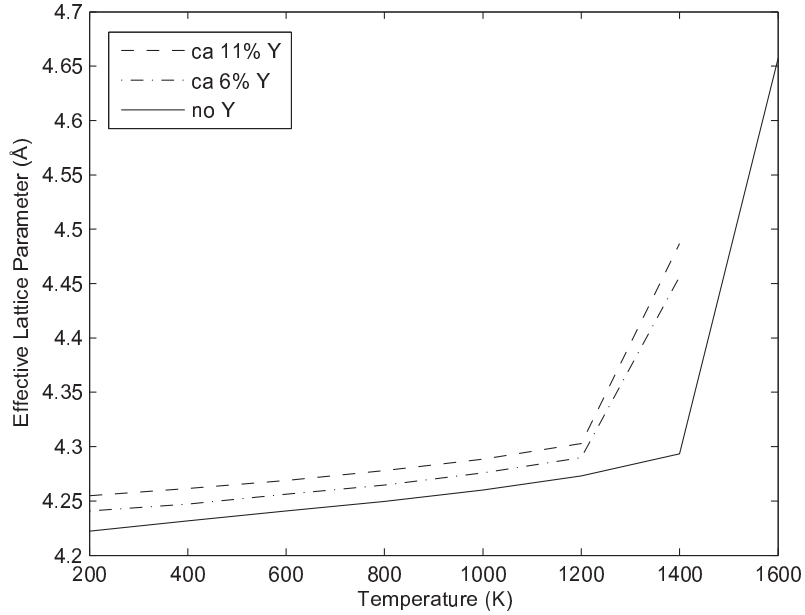


**Figure 6.3:** The lattice parameter as a function of temperature, plotted for three yttrium dopant concentrations, 11 %, 6 % and no doping at all.

shows a large increase from 1200 K to 1400 K and a similar increase is also seen for the undoped lattice from 1400 K to 1600 K.

To study the behavior for temperatures up to 1200 K a second order polynomial fit was made for each of the three curves at the temperatures 200 K to 1200 K and the resulting effective lattice parameters as functions of temperature are

$$d_{11Y} = 2.55 \cdot 10^{-8}T^2 + 1.12 \cdot 10^{-5}T + 4.25, \quad (6.2)$$

$$d_{6Y} = 2.36 \cdot 10^{-8}T^2 + 1.55 \cdot 10^{-5}T + 4.24, \quad (6.3)$$

$$d_{0Y} = 1.22 \cdot 10^{-8}T^2 + 3.30 \cdot 10^{-5}T + 4.22, \quad (6.4)$$

where the index denotes the yttrium dopant concentration, the temperature  $T$  is in Kelvin and the effective lattice parameter  $d$  is in Ångström.

A plot containing the data points and the second order polynomial fit is shown in figure 6.4. The constant term increases with dopant concentration, highlighting an increase of the lattice parameter as a function of dopant concentration. The second order fit seem to be a good match to the data points. Further, by studying equation 6.2-6.4 it is clear that the second order temperature dependence increases with doping and the linear dependence decreases.

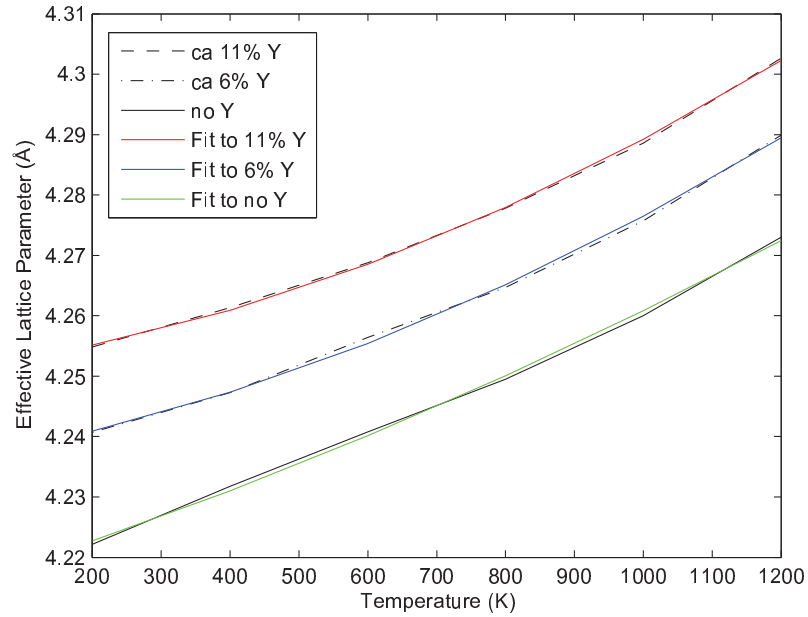


**Figure 6.4:** The lattice parameter as a function of temperature, plotted for three yttrium dopant concentrations, 11 %, 6 % and no doping at all. Included in the graph is a also the second order polynomial fit to each curve.

A second order thermal expansion was found for undoped barium zirconate in experiments performed by Zhao *et al*[15], the results in equation 6.4 shows a second order term that is a factor 1.1 larger and a first order terms that is a factor 1.5 larger than their results.

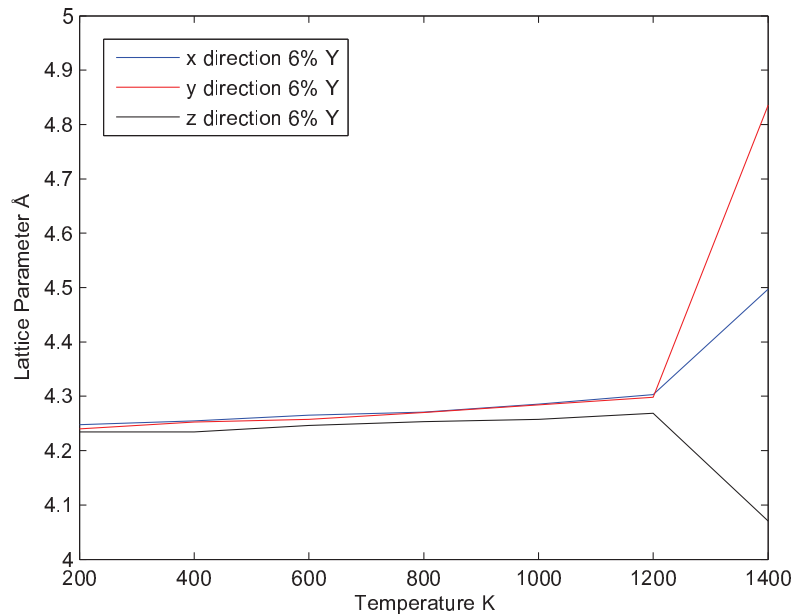


**Figure 6.5:** The lattice expansion in the  $x$ ,  $y$  and  $z$ -directions for 6% yttrium doped barium zirconate. The graph shows a slight tetragonal distortion, except for 1400 K where the lattice becomes strongly orthorhombic.

## 6.2.2 Distortions From the Cubic Lattice Structure

The simulation volume was allowed to change shape during the MD simulations, meaning that the axes,  $x$ ,  $y$  and  $z$ , were allowed to change length separately. Figure 6.5 and 6.6 shows the lattice parameter in the  $x$ ,  $y$  and  $z$ -directions for 6% and 11% yttrium dopants as a function of temperature. The graphs are rather similar but there are some differences worth pointing out. For 6% yttrium doped barium zirconate a slight tetragonal distortion can be seen, where the  $z$ -direction lattice parameter is a little bit smaller than the other two which are very similar. A tetragonal distortion for 6% yttrium doped lattices has been found experimentally by Giannici *et al* [11], where two sides are slightly longer than the third. For 11% yttrium dopants there is an orthorhombic distortion instead of tetragonal one, with all sides being of different length. In both of the doped cases the distortion from a cubic lattice is very small for temperatures below 1400 K.

Figure 6.3 shows a large increase in the effective lattice parameter from 1200 K and 1400 K. Figure 6.5 and 6.6 shows that not only does the simulation volume become larger, but the lattices does also become clearly orthographically distorted. The experimental data found does not cover these temperatures so it is difficult to say weather this is a real physical phenomena or an artifact from the potential.

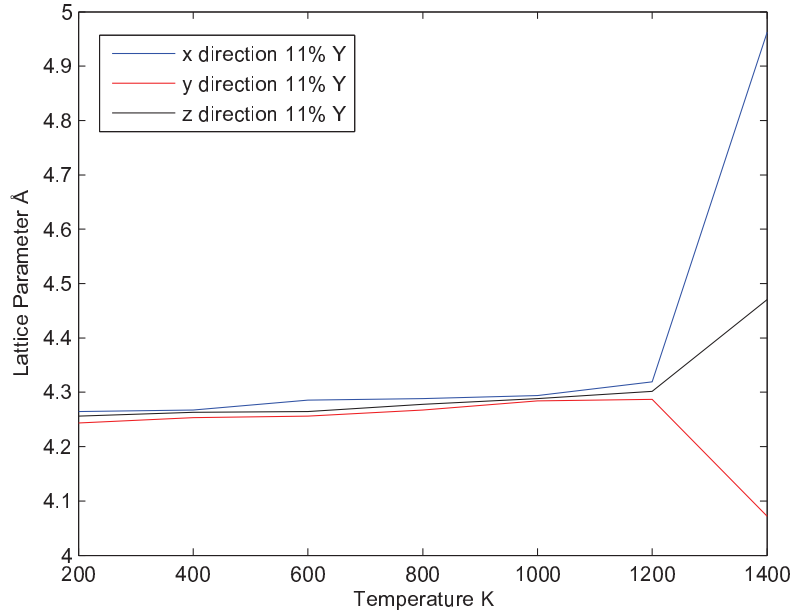


**Figure 6.6:** The lattice expansion in the  $x$ ,  $y$  and  $z$ -directions for 11% yttrium doped barium zirconate. The graph shows a slight orthorhombic distortion, except for 1400 K where the lattice becomes strongly orthorhombic.

## 6.3 Proton Diffusion in Yttrium Doped Barium Zirconate

The study of proton diffusion was made in systems of  $6 \times 6 \times 6 = 216$  unit cells with periodic boundary conditions. The systems contained 11% yttrium dopants, were neutrally charged and fully protonated, meaning the systems contained 24 yttrium atoms, 24 protons and no oxygen vacancies. As in the case of the lattice expansion study in the previous section, the dopants and protons were distributed by randomly replacing zirconium atoms with yttrium and randomly selecting the starting positions for the protons. In all simulations the simulation volume was kept constant and cubic with a fixed lattice parameter with the temperature dependence obtained in the lattice expansion simulations. The systems were relaxed before the MD simulations were started and the time step was  $\Delta t = 1$  fs.

### 6.3.1 Mean Square Displacement

The temperature dependence of the diffusion constant was investigated. A simulation was made for seven different temperatures 800–1400 K with a temperature step of 100 K. Due to the uncertainty of the behavior at higher temperatures, the lower temperature behavior of the lattice parameter was extrapolated when performing MD simulations at 1300 and 1400 K. The simulations each contained  $5 \cdot 10^5$  time steps, corresponding to

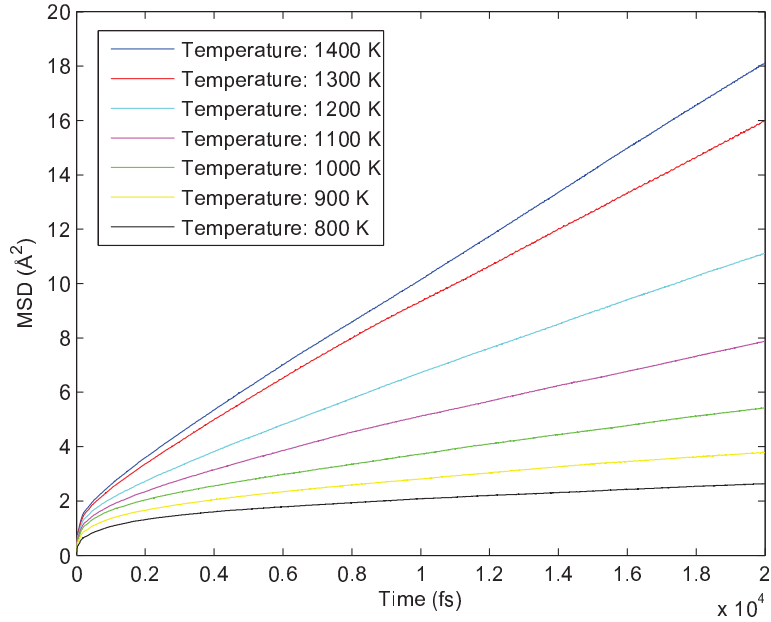


**Figure 6.7:** The mean square displacement for a proton diffusing in 11 % yttrium doped barium zirconate, at the seven temperatures 800 K to 1400 K.

0.5 ns. The diffusion constant was calculated for each simulation, following the MSD procedure in section 5.1.1. The number of time windows used for averaging in the MSD calculations are close to 4000 and the average has also been taken over the 24 protons.

The averaged MSD plots are shown in figure 6.7. The resulting temperature dependence of the diffusion constant is shown in figure 6.8.

Figure 6.7 clearly shows how the MSD becomes linear after about 5 ps and allows for a determination of the diffusion constant by fitting of a first order polynomial to the second half of the curve.

Using equation 3.6 in section 3.3 it is possible to determine the activation energy  $E_0$  and the prefactor  $D_0$ . By taking the logarithm of both sides of equation 3.6 and extracting the factor  $1000/T$ , the result becomes the first order polynomial

$$\ln D = -\frac{1000}{T} \frac{E_0}{1000k_B} + \ln D_0, \quad (6.5)$$

where  $\ln D$  is a function of  $1000/T$ .

By making a first order polynomial fit to the data points from 800 K to 1400 K,  $E_0 = 0.44$  eV can be extracted from the slope of the curve and  $D_0 = 5.3 \cdot 10^{-4}$  cm<sup>2</sup>/s from the constant term. The activation energy is well in agreement with experiments performed by Kreuer *et al*[4], but the prefactor is about a factor five too small. The experimental data is shown as a fully drawn line in figure 6.8. The prefactor is however about a factor two larger than the one van Duin *et. al.* obtained in their study of the

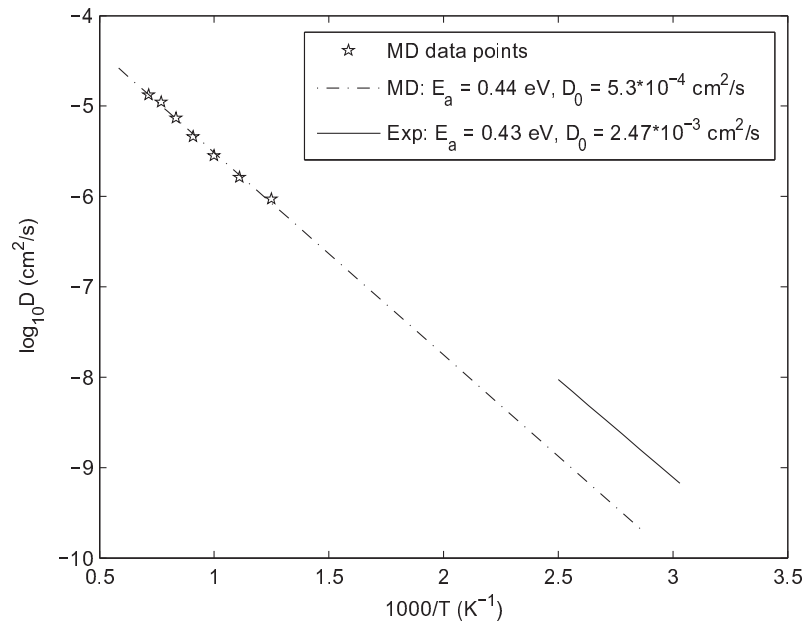


**Figure 6.8:** The diffusion constant for protons in 11 % yttrium doped barium zirconate, as a function of temperature. The dashed line is a fit to the data obtained from the MD simulations and the fully drawn line corresponds to the result from experiments performed by Kreuer *et al*[4].

diffusion in barium zirconate[7].

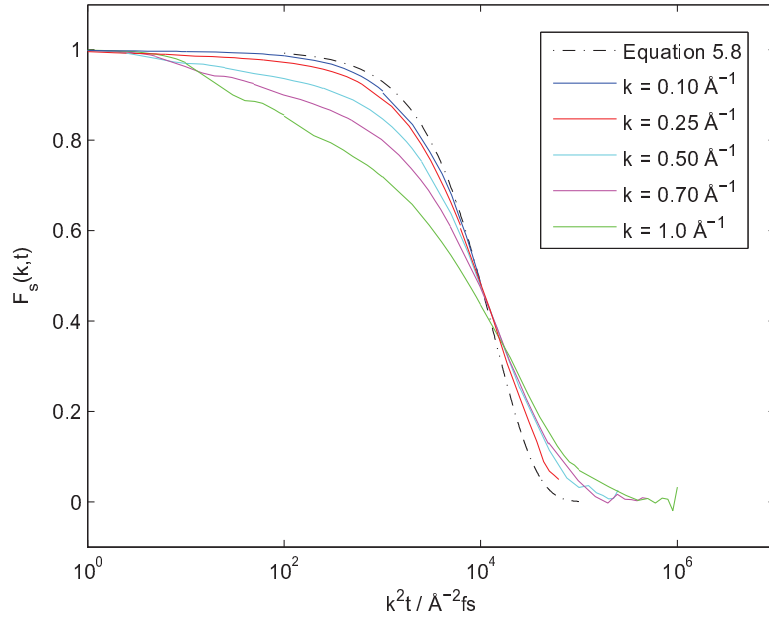


**Figure 6.9:** The s-ISF as a function of  $k^2t$  for some  $k$ -values between  $k = 0.1 \text{ \AA}^{-1}$  and  $k = 1 \text{ \AA}^{-1}$ . The dotted line is the exponential function from equation 5.8, with  $D = 7.3 \cdot 10^{-6} \text{ cm}^2/\text{s}$ .

### 6.3.2 Self Intermediate Scattering Function

The s-ISF was obtained for a system simulated at 1200 K, where the self diffusion constant was calculated to be  $D = 7.3 \cdot 10^{-6} \text{ cm}^2/\text{s}$ , or  $\log_{10}D = -5.14$ , with the MSD method. The simulation contained  $5 \cdot 10^6$  time steps, corresponding to 5 ns. The s-ISF was calculated using the procedure in section 5.1.2. 1200 K is above the intermediate temperature range but the elevated temperature is necessary to increase the speed of the dynamics, otherwise it would take a very long time to perform a simulation long enough to capture the behavior of interest.

The calculated s-ISF as a function of  $k^2t$  is shown in figure 6.9. For some  $k$ -values between  $k = 0.1 \text{ \AA}^{-1}$  and  $k = 1 \text{ \AA}^{-1}$ . The s-ISF for small  $k$ -values, equation 5.8 in section 5.1.2, is also included in figure 6.9, with  $D = 7.3 \cdot 10^{-6} \text{ cm}^2/\text{s}$ .

The curves in figure 6.9 approaches the exponential behavior in equation 5.8 for small  $k$  but even the smallest value  $k = 0.1 \text{ \AA}^{-1}$  does not seem to reproduce the exponential behavior completely. For larger  $k$ -values the graph drops rapidly before it becomes more exponential in appearance. This behavior is expected because  $k = 1 \text{ \AA}^{-1}$  corresponds to the distance  $r = 2\pi/k \approx 6.3 \text{ \AA}$ , which is close to the size of the unit cell, and therefore are the small vibrational movements of the protons captured. To extract more information

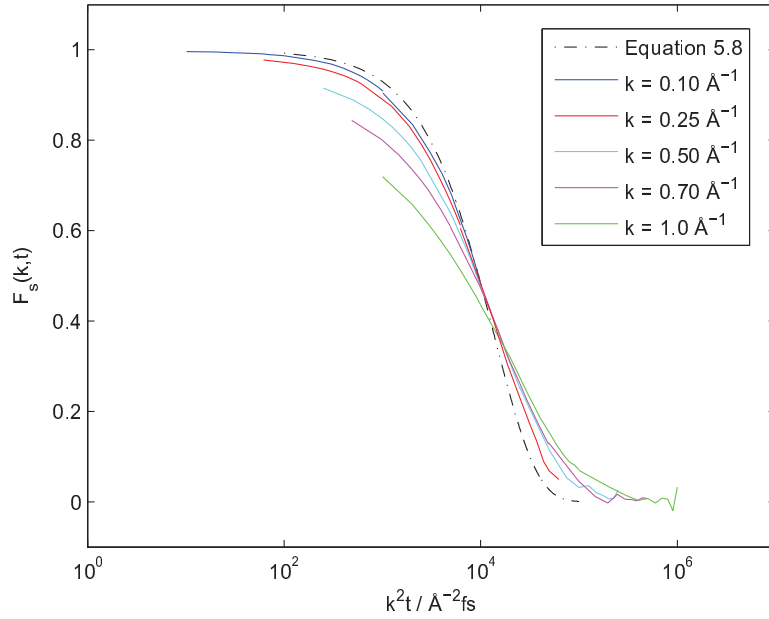


**Figure 6.10:** The part of the self ISF as a function of  $k^2t$  that were fitted to the expression in equation 6.6. The plot shows some  $k$ -values between  $k = 0.1 \text{ \AA}^{-1}$  and  $k = 1 \text{ \AA}^{-1}$  but the fit where made for 600  $k$ -values between  $k = 0.1 \text{ \AA}^{-1}$  and  $k = 1 \text{ \AA}^{-1}$ . The dotted line is the exponential function from equation 5.8, with  $D = 7.3 \cdot 10^{-6} \text{ cm}^2/\text{s}$ .

about the  $k$ -dependence of the s-ISF a fit was made to the expression

$$F_s(k,t) = F_0 e^{-\left(\frac{t}{\tau}\right)^\beta}, \quad (6.6)$$

where the parameters are  $k$ -dependent,  $F_0 = F_0(k)$ ,  $\tau = \tau(k)$  and  $\beta = \beta(k)$ . Equation 6.6 is a so called stretched exponential in  $t$  and has a rather complex  $k$ -dependence. The  $x$ -axis in figure 6.9 is in  $k^2t \text{ \AA}^{-2}\text{fs}$  so the parameter that was actually fitted was  $D'(k) = 1/(\tau(k)k^2)$  instead of  $\tau$ .

The fit was made to the part of the data where the behavior could be replicated by the expression in equation 6.6, meaning that the fit does not include the drop that occurs for larger  $k$ -values. The part of the s-ISF that was used to fit the data is shown in figure 6.10.

To reproduce the simple exponential behavior in equation 5.8, the expressions

$$F_0(k) \rightarrow 1, \text{ when } k \rightarrow 0, \quad (6.7)$$

$$\log_{10} D'(k) \rightarrow \log_{10} D = -5.14, \text{ when } k \rightarrow 0 \text{ and} \quad (6.8)$$

$$\beta(k) \rightarrow 1, \text{ when } k \rightarrow 0 \quad (6.9)$$

should hold.

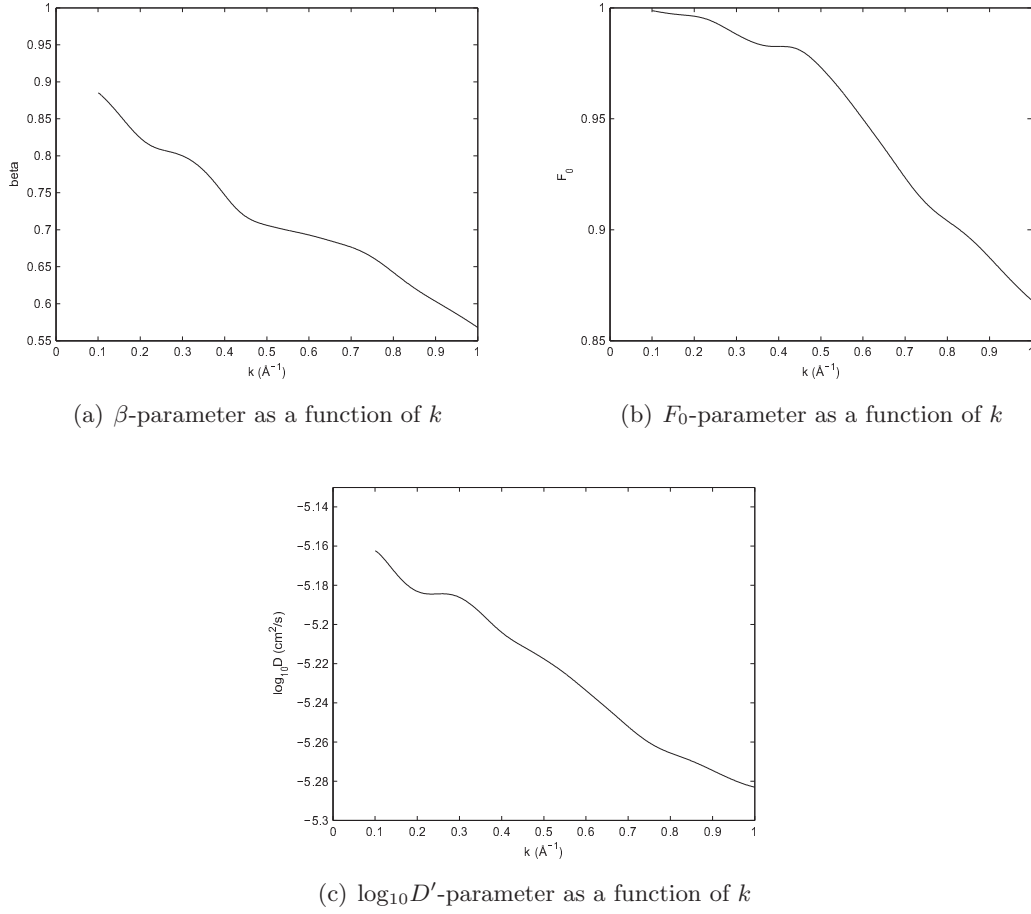


**Figure 6.11:** The parameters  $\beta$ ,  $F_0$  and  $\log_{10} D'$  as a function of  $k$ , where  $k$  goes from  $0.1 \text{\AA}^{-1}$  to  $1 \text{\AA}^{-1}$ .

The parameters  $\beta$ ,  $F_0$  and  $\log_{10} D'$  are plotted as a function of  $k$  in figure 6.11.

It is difficult to interpret the results in figure 6.11 because there are no known theoretical predictions for this behavior.

The fit seem to reproduce the flattening of the curves for larger  $k$ , which corresponds to a decrease in the  $\beta$ -parameter in figure 6.11(a). Due to the drop in the s-ISF for larger  $k$  the fitted curve is shifted downwards which is shown as a decrease in the prefactor  $F_0$  in figure 6.11(b) for larger  $k$ . From figure 6.11(c) it is possible to see that the  $D'$ -parameter clearly decreases with increasing  $k$ .

# 7

## Discussion

THE ACCURACY OF the parametrization of the ReaxFF potential was investigated by using it to calculate the energy difference between seven different structures and comparing the difference to DFT calculations for the same structures. The difference between the ReaxFF calculated values and the DFT calculated ones are about 1 – 10 kJ/mol, except for one structure where the difference is around 40 kJ/mol. The energy values calculated with the ReaxFF potential seem to follow the trend of the values calculated with DFT and the agreement in energy is adequate. The same structures were compared in reference [7], but the DFT calculated values differs somewhat. The difference is most likely due to that the DFT calculations performed in reference [7] used Gaussian basis functions and the calculations performed during this thesis used a plane wave basis, another difference is the pseudopotentials used.

The results of the thermal expansion investigation of undoped barium zirconate agree rather well with experimental data for temperatures up to 1200 K. The expansion of the lattice as a function of temperature is slightly overestimated, the second order being a factor 1.1 larger and the first order a factor 1.5 larger than experiments performed by Zhao *et al*[15]. The overestimated expansion is consistent with observations made by Raiteri *et al*[27], that the ReaxFF potential that models barium zirconate is too soft. The doped lattices investigated in this thesis show a slight distortion from the cubic structure. For 6% yttrium dopants the distortion is tetragonal which is in agreement with experiments performed by Giannici *et al*[11]. For 11% yttrium dopants the distortion is orthorhombic and this has not been observed experimentally so it can be an artifact from the potential.

At higher temperatures a much larger increase in the lattice parameter is observed and the distortion of the doped lattices becomes highly orthorhombic, this has not been observed experimentally. The distortion is most likely due to an inaccuracy of the ReaxFF potential. Raiteri *et al*[27] observed that the ReaxFF potential has instabilities and predicts an unphysical distortion for undoped barium zirconate, perhaps this flaw

becomes more evident at higher temperatures.

Proton diffusion in barium zirconate seems to be well modeled by the ReaxFF potential and it seems like it is possible to model proton diffusion at higher temperatures if the system size is kept fixed with a lattice parameter extrapolated from the lower temperature behavior. The activation energy  $E_0 = 0.44$  eV is in very good agreement with reported experimental results and the prefactor  $D_0 = 5.3 \cdot 10^{-4}$  cm<sup>2</sup>/s is about a factor 5 too small. It is difficult to state the reason for the deviation in  $D_0$ .  $D_0$  depends on several factors and a deviation of a factor of 5 can still be considered to be a good result. It is worth mentioning that no quantum mechanical effects for the motion of the atoms are taken into account during a MD simulation, which may affect the result. Also, there may be errors to be considered in the experimental data as well.

The main topic of this thesis has been  $F_s(\mathbf{k}, t)$ , the self intermediate scattering function (s-ISF), and in particular has the  $k$ -dependence of the s-ISF been investigated. The behavior of the s-ISF can be well replicated by a stretched exponential function in time but with three  $k$ -dependent parameters. The s-ISF approaches an exponential function for small values of  $k$ , which is predicted by theory. However, even for  $k$ -values as small as  $0.1 \text{ \AA}^{-1}$ , the s-ISF deviates from the exponential time dependence.  $k = 0.1 \text{ \AA}^{-1}$  corresponds roughly to distances of the order of  $r = 2\pi/k \approx 60 \text{ \AA}$  and the observed deviation may indicate that the diffusive motion is affected by the dopants.

The s-ISF describes "diffusion" at different length scales and might give information about trapping in the vicinity of the dopants. To investigate this further it would be necessary to investigate the trajectory files more closely and map the motion of the protons through out the lattice in space and time.

It would be advantageous to do simulations over longer time intervals but the computational power of computers and the MD method puts an upper limit to how long time intervals that can be studied in practice. Due to the fact that the MD simulation time is finite the maximal value of  $k^2 t$  becomes smaller as  $k$  decreases. When  $k = 0.1 \text{ \AA}^{-1}$  the  $(k^2 t)_{max} = 50 \text{ \AA}^{-2}$  ps for a time interval of 5 ns, which is just a small part of the exponential curve. Also, for lower temperatures, the kinetics are slower and therefor are longer simulation times required to study lower temperatures.

# 8

## Conclusions

THE DIFFUSION OF protons seems to be well modeled by the ReaxFF potential and the results are close to the ones obtained from experiments. The self intermediate scattering function can be obtained for both large and small values of the momentum  $|k|$  and could prove to be a useful tool in the investigation of the effects of dopants.

There are a lot more to be done on this topic. The next step would be to look at trajectory files and investigate the motion of protons in space and time. More MD simulations could be performed at lower temperatures to investigate the behavior in the intermediate temperature range and longer simulations in time could be useful to increase the amount of data that can be used to fit parameters to. It would be useful to obtain more experimental data for the s-ISF and compare these to the results obtained for different  $k$ -values in this thesis.

The ReaxFF potential can be improved. Improving the potential is however a difficult task due to the complexity of it. The potential can be used with good results if high temperatures are avoided. However, it seems that higher temperatures can be studied if the size is kept fixed and the lattice parameter is extrapolated from the lower temperature behavior.

# Bibliography

- [1] Minh, Nguyen Q., 1993. Ceramic fuel cells. *Journal of the American Ceramic Society*, 76 (3) , pp. 563-588
- [2] Ormerod, R.M., 2003. Solid oxide fuel cells. *Chemical Society Reviews*, 32 (1) , pp. 17-28
- [3] Tarancón, A., 2009. Strategies for lowering solid oxide fuel cells operating temperature. *Energies*, 2 (4) , pp. 1130-1150
- [4] Kreuer, K.D., 2003. Proton-Conducting Oxides. *Annual Review of Materials Research*, 33 , pp. 333-359
- [5] Karlsson, M., Engberg, D., Björketun, M.E., Matic, A., Wahnström, G., Sundell, P.G., Berastegui, P., Ahmed, I., Falus, P., Farago, B., Börjesson, L., Eriksson, S., 2010. Using neutron spin-echo to investigate proton dynamics in proton-conducting perovskites. *Chemistry of Materials*, 22 (3) , pp. 740-742
- [6] Frenkel, D., Smit, B., 2002. *Understanding Molecular Simulation - 2nd ed.* Academic Press 84 Theobald's Road, London WC1X 8RR, UK
- [7] Van Duin, A.C.T., Merinov, B.V., Han, S.S., Dorso, C.O., Goddard III, W.A., 2008. ReaxFF reactive force field for the Y-doped BaZrO<sub>3</sub> proton conductor with applications to diffusion rates for multigranular systems. *Journal of Physical Chemistry A*, 112 (45) , pp. 11414-11422
- [8] LAMMPS Molecular Dynamics Simulator, 2012, <http://lammps.sandia.gov/> LAMMPS is distributed as a free open source code and is distributed by Sandia National Laboratories, a US Department of Energy laboratory.
- [9] Larminie, J. & Dicks, A., 2003. *Fuel Cell Systems Explained - 2nd ed.* John Wiley & Sons Ltd, Chichester.
- [10] Schroeder, D., 2000. *Introduction to Thermal Physics*. Addison Wesley Longman.

- 
- [11] Giannici, F., Shirpour, M., Longo, A., Martorana, A., Merkle, R., Maier, J., 2011. Long-range and short-range structure of proton-conducting Y:BaZrO<sub>3</sub>. *Chemistry of Materials*, 23 (11) , pp. 2994-3002
- [12] Colomban, P., Zaafrani, O., Slodczyk, A., 2012. Proton content and nature in perovskite ceramic membranes for medium temperature fuel cells and Electrolysers. *Membranes*, 2 (3) , pp. 493-509
- [13] Ishihara, T., 2009. *Perovskite Oxide for Solid Oxide Fuel Cells* Springer Science+Business Media, LLC, 233 Spring Street, New York, NY 10013, USA.
- [14] Charrier-Cougoulic, I., Pagnier, T., Lucazeau, G. 1999. Raman Spectroscopy of Perovskite-Type BaCe<sub>x</sub>Zr<sub>1-x</sub>O<sub>3</sub>(0 ≤ x ≤ 1). *Journal of Solid State Chemistry* 142 (1) , pp. 220-227
- [15] Zhao, Y., Weidner, D.J., 1991. Thermal expansion of SrZrO<sub>3</sub> and BaZrO<sub>3</sub> perovskites. *Physics and Chemistry of Minerals* 18 (5) , pp. 294-301
- [16] Björketun, M.E., Sundell, P.G., Wahnström, G., Engberg, D., 2005. A kinetic Monte Carlo study of proton diffusion in disordered perovskite structured lattices based on first-principles calculations. *Solid State Ionics* 176 (39-40) , pp. 3035-3040
- [17] Cammarata, A., Ordejón, P., Emanuele, A., Duca, d., 2012. Y:BaZrO<sub>3</sub> Perovskite Compounds I: DFT Study on Unprotonated and Protonated Local-Structure. *Chemistry - An Asian Journal* 7 (8) , pp. 1827-1837
- [18] Cammarata, A., Ordejón, P., Emanuele, A., Duca, d., 2011. Y:BaZrO<sub>3</sub> Perovskite Compounds II: Designing Protonic Conduction by MD Models. *Chemistry - An Asian Journal* 7 (8) , pp. 1838-1844
- [19] Björketun, M.E., Sundell, P.G., Wahnström, G., 2007. Effect of acceptor dopants on the proton mobility in BaZr O<sub>3</sub>: A density functional investigation. *Physical Review B - Condensed Matter and Materials Physics* 76 (5) , art. no. 054307
- [20] Allen, M.P., Tildesley, D.J., 1987. *Computer Simulation of Liquids*. Oxford University Press, Walton Street, Oxford OX2 6DP.
- [21] Thijssen, J.M., 1999. *Computational Physics - 2nd ed.* Cambridge University Press, The Edinburgh Building, Cambridge CB2 8RU, UK.
- [22] Tuckerman, M., Berne, B.J., Martyna, G.J., 1992. Reversible multiple time scale molecular dynamics. *The Journal of Chemical Physics* 97 (3) , pp. 1990-2001
- [23] Bée, M., 1988. *Quasielastic neutron scattering* Adam Hilger imprint by IOP Publishing Ltd, Techno House, Redcliffe Way, Bristol BS1 6NX, England.
- [24] MATLAB, 2013, <http://www.mathworks.se/products/matlab/>
- [25] dynsf, 2012, <http://code.google.com/p/dynsf/>

- [26] Yamanaka, S., Kurosaki, K., Maekawa, T., Matsuda, T., Kobayashi, S.-I., Uno, M., 2005. Thermochemical and thermophysical properties of alkaline-earth perovskites. *Journal of Nuclear Materials* 344 (1-3) , pp. 61-66
- [27] Raiteri, P., Gale, J.D., Bussi, G., 2011. Reactive force field simulation of proton diffusion in BaZrO<sub>3</sub> using an empirical valence bond approach. *Journal of Physics Condensed Matter* 23 (33) , art. no. 334213